Feed-Forward Voltage Photovoltaic Battery Dc Microgrid Control Using an Enhanced Seeker Optimization Algorithm

[1] K.Sushmitha, PG Student,[2] M.Sreenivasulu
Electrical and Electronics Engineering
[1,2] Gokula Krishna College of Engineering, Sullurupet

Abstract: **A novel power system supply architecture that may efficiently use renewable energy sources and work with contemporary DC electrical equipment is the photovoltaic-battery DC.In order to increase PV usage and bus voltage performance, this study proposes a quick and effective maximum power point tracking (MPPT) photovoltaic (PV) control method as well as a battery energy storage system (BESS) bus control approach.First, the mathematical model of each distributed generation in the DC microgridis derived after the photovoltaic-battery and power balance principles are examined. Second, by adding the time-varying smoothing factor and voltage increase, the exponential variable step perturbation and To speed up the MPPT process, an observation method for PV controllers is suggested.The enhanced seeker optimization algorithm (ISOA) optimizes the BESS voltage controller's parameters in light of the significant power fluctuation on the DC bus and the periodic disruption of PV energy absorption. enhanced by the chaotic initialization optimization approach and the variational Cauchy operator.enhanced by the chaotic initialization optimization approach and the variational Cauchy operator.Additionally, a feed-forward compensation approach is created to decrease the hysteresis features and increase the voltage closed-loop reaction speed. Lastly, MATLAB/Simulink is used to implement multi-scheme simulation studies. . The suggested approach increases the MPPT reaction speed from 70 ms to 10 ms and lowers the average voltage ripple percentage from 3% to 1% when compared to the experimental findings of the conventional control method. The outcomes of the experiment confirmed the accuracy and potency of the suggested approach.**

Terms Index: **PID control, seeker optimization method, DC microgrid, voltage stabilization control, and tracking of the maximum power point.**

I.INTRODUCTION

A useful renewable energy structure, the photovoltaic-battery DC microgrid is flexible in addressing DC requirements and highly efficient at absorbing PV energy demand.PV power and adaptability in supplying DC needs. Additionally, it is getting more attention [1–3]. A power electronic converter connects the PV system and BESS to the DC bus in a photovoltaic-battery DC microgrid.To utilize more renewable energy, the PV system is often set up as the main power supply and the BESS as an auxiliary power supply, which maintains the power balance in the DC microgrid and suppresses fluctuations in the DC bus voltage by charging and discharging.However, the intricate problems of reactive power, frequency fluctuation, phase synchronization, and tide current do not need to be taken into account by DC microgrids. One of the key areas of study for photovoltaic-battery DC microgrids is the high-performance bus voltage control technique.due to the complicated intermittent features of PV systems, the extremely non-linear properties of power electronic systems, and the load demand that fluctuates at random [4-6].

Because traditional technologies are not robust to complicated changes in sunlight intensity and surroundings, they make it difficult to meet the power supply requirements of dynamic loads. To guarantee dynamic robust stability of the DC bus voltage, power management and non-linear control techniques must be developed using the dynamic mathematical model of the power electronic interface converter as well as the output characteristics of each source. For instance In order to maintain the bus voltage and satisfy load demand, reference [7] suggests a DC micro grid architecture for PV and BESS and creates an energy management plan for ideal power flow. In order to preserve the stability of the bus voltage, Reference [8] A nonlinear local state feedback controller that can efficiently control voltage stability is proposed in Reference [12], although it is only applicable to microgrids with constant loads. A fuzzy logic-based PL-PI controller for DC bus voltage control and regulation is proposed in Reference [13]. However, it has the issue of choosing parameters that are challenging. A controller based on the backstepping technique is suggested in Reference [14], which can significantly increase the system's resilience but has minor issues with stability and voltage balancing.suggests an isolated DC microgrid structure with PV, a diesel generator, and BESS. The energy management of all three components is utilized. In order to achieve power balance and voltage stability in the network, Reference [7-8] focuses on the steady state equations of each source and uses the average energy model computation to regulate each source's output. Because intermittent output is a feature of renewable energy, controller design is crucial. In order to balance power dynamics and stabilize bus voltage, Reference [9] suggests a combined approach that uses the centralized fuzzy logic control method and the gain scheduling method for DC bus voltage management regulation. Even while fuzzy control is simple to use, its accuracy and logical rules still require refinement. A model predictive voltage control approach that designs closed-loop voltage control rules using a power linearization model was presented in Reference [10]. In terms of adaptability to a broad operating range and robustness to suppress external uncertainties, the predictive controller based on linear models is inadequate due to its restricted operating range and accurate model parameter identification. An Active Disturbance Rejection Control (ADRC) is suggested in Reference [11] to regulate the charging and discharging of DC bus voltages and BESS. Although ADRC's robustness in managing model parameters and outside disturbances is a benefit, its selection and control procedures require optimization. The use of parameter tweaking in algorithms has emerged as a viable and successful strategy with the advancement of computational tools. The settings of PID controllers are controlled by a variety of algorithms, including particle swarm optimization (PSO) methods in [17], ant colony optimization (ACO) strategies in [16], and genetic algorithms (GA) in [15]. While the local search capability in the GA is poor and frequently takes a long time to obtain the optimal answer, the global search capability is powerful enough to locate the sub-optimal solution rapidly. ACO's complicated parameter configuration makes it simple to stray from the ideal result if the parameters are not set correctly. Due to its propensity to induce early convergence and fall into local optimum solutions, PSO is ineffective in real-world manufacturing.

The seeker optimization method (SOA) [18] has the advantages of fast convergence, great search capability, and simplicity of principle as compared to the numerous optimization techniques mentioned above, but it still has thedrawbacks of early search speed reduction and the propensity to settle into a local optimum. Some academics have suggested incorporating chaos theory into optimization algorithms as a solution to this issue [19]. Randomness, ergodicity, and regularity are characteristics of the chaotic initialization that can significantly enhance the algorithm's convergence performance and solution accuracy. In order to increase control reaction speed, steady-state accuracy, and robustness under challenging photovoltaic-battery operating conditions, this research attempts to construct a high-performance control system with an optimal parameter tuning function. In the modern industrial control environment, the proportional-integral-differential control approach is one of the most widely used and dependable classical control techniques. Strong stability, robustness, adaptability, simplicity, and ease of implementation are the benefits of the PID controller. In nearly real-time, it can monitor and modify the controlled system states based on feedback. In order to accommodate a variety of settings and needs, it can also easily adjust the control parameters in accordance with various real-world circumstances. However, because parameter turning is a complex operation, the control parameters are frequently chosen badly, which results in subpar output performance. This work enhances the SOA by adopting a chaotic initiation method and variational Cauchy operator to improve the bus voltage performance of the photovoltaic-battery DC microgrid.The PID controller's parameters are optimized by the use of the enhanced SOA (ISOA). The DC bus voltage control reaction speed, accuracy, and robustness are increased by further using the feed-forward control approach to suppress disturbances. In conclusion, this paper's primary contributions are as follows: (1) The mathematical model of the PV system and BESS in the DC microgrid is derived, and the principle of photovoltaic-battery and power balancing is examined. (2) To increase operation efficiency, the MPPT PV controller with exponential variable step perturbation and observation technique is created by adding the PV voltage increment and time-varying smoothing factor.. (3) The ISOA optimizes the BESS voltage controller's parameters in light of the significant power fluctuations on the DC bus and the sporadic disruption of PV energy absorption. (4) To achieve the dynamic stabilization control of bus voltage and the acceptable distribution of photovoltaic-battery power, a DC bus voltage feed-forward controller is designed for BESS.(5) Multi-scheme MATLAB/Simulink digital simulation is used to confirm the accuracy and efficacy of the suggested control system. The structure of the paper is as follows: The mathematical modeling and operation of the photovoltaic-battery DC microgrid are explained in Section II. The ISOA-PID voltage controller for BESS and the MPPT controller for PV systems are designed in Section III, respectively. Section IV designs three operation circumstances, four simulation schemes, and evaluates the accuracy and efficacy of the control strategy put forth in this work. are confirmed by the results of the simulation comparison. Section V concludes with a description of the research findings and directions for future research in this publication.

II. OPERATION AND MATHEMATICAL CONSTRUCTION OF PHOTOVOLTAIC-BATTERY DC MICROGRID'S

A. Photovoltaic-battery DC microgrid architecture

The general layout of the photovoltaic-battery DC microgrid, including the PV system, BESS, and DC load, is depicted in Fig. 1. The PV output power, BESS output power, load power, and total bus power are denoted as P_{pv}, P_{bess} , P_{load} and P_{net}, respectively. The bus voltage and bus equivalent capacitance are denoted by V_{dc} and C_{dc}, respectively. The PV system is set up as a power main supply and connected to the common DC bus via a DC-DC boost converter in order to optimize the use of renewable energy. A bi-directional DC-DC converter connects the BESS, an energy storage and stabilization power supply, to the DC bus. The BESS transfers electricity to the DC microgrid during periods of high load and stores extra energy produced by the PV system during periods of intense sunlight. It uses quick charge and discharge regulation to keep the bus voltage dynamically stable.

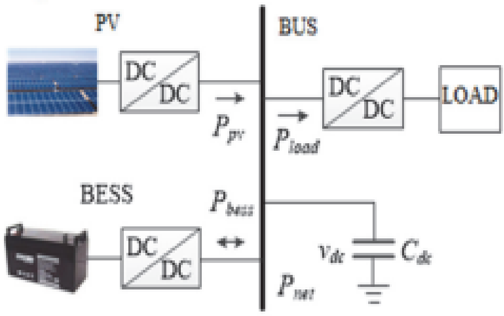

Figure. 1 shows a typical DC microgrid system structure.

B.A DC bus power balancing principle:

The total power P_{net} balancing equation of the photovoltaic-battery DC microgrid can be written as follows using the power conservation principle:

$$P_{net} = P_{pv} + P_{bess} - P_{load} \tag{1}$$

The PV system provides the microgrid with positive power while operating in MPPT power generation mode. When charging, the BESS output power is negative, and when manner of discharge. The main responsibility for guaranteeing stable microgrid operation under all operating conditions is maintaining a steady DC bus voltage. Thus, the input-output power on the bus stays at zero, or P_{net}=0, under steady-state constant voltage conditions. The power-voltage relationship under dynamic situations can be stated as follows:

$$v_{dc}\frac{dv_{dc}}{dt} = \frac{1}{C_{dc}}P_{net} \tag{2}$$

To maintain the stability of the DC bus voltage, the BESS's charging and discharging must bemanaged in accordance with power variations.

C.The PV system's mathematical model :

The PV system is typically made up of numerous separate PV cells coupled in parallel and series. In order to match the PV array's output voltage with the DC microgrid common bus voltage, these PV cells combine to form a PV array and employ a DC-DC boost converter [20]. Fig. 2 depicts a PV system's comparable circuit.

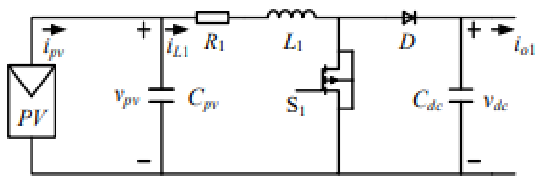

Figure 2: PV system equivalent circuit

The PV array output voltage, filter capacitor, and output current are denoted as V_{pv}, C_{pv}, and i_{pv} in Figure 2, respectively. R_1, D, L_1, and iL_1 are the boost converter resistor, diode, inductor, and inductor current, respectively. The DC system equivalent load current is denoted by i_{o1}. Given that the power electronic switch S_1's duty cycle control quantity is μ_1, the mathematical model of the PV system seen in Fig. 2 can be represented as [21] using Kirchhoff's circuit rule.

$$\begin{cases} \dot{v}_{pv} = \frac{1}{C_{pv}}\left(i_{pv} - i_{L1}\right) \\ \dot{i}_{L1} = \frac{1}{L_1}\left(-R_1 i_{L1} + v_{pv} - (1-\mu_1)v_{dc}\right) \\ \dot{v}_{dc} = \frac{1}{C_{dc}}(1-\mu_1)i_{L1} - \frac{1}{C_{dc}}i_{o1} \end{cases} \quad (3)$$

A DC-DC boost converter connects the PV array to the DC bus. Because solar power is sporadic, the MPPT technique is frequently used to regulate the boost converter, resulting in a Constant Power Source (CPS) as the PV system's output.

D. The BESS's mathematical model

Fig. 3 depicts the equivalent circuit for the battery bank and bi-directional DCDC converter that make up the BESS.

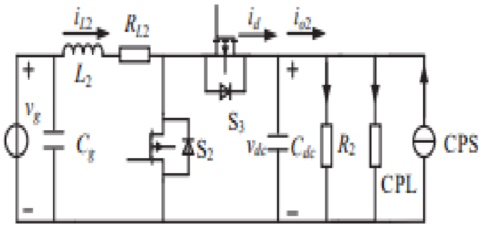

Figure 3: The BESS's equivalent circuit

The BESS battery bank output terminal voltage (Vg) and filter capacitance (Cg) are shown in Fig. 3. L_2, RL_2, and iL_2 represent the inductor, parasitic resistance of the inductor, and the bi-directional DC-DC converter's inductor current, accordingly. The current passing through the power electronic switch S_3 is denoted by id. The DC system equivalent load current is denoted by i_{o2}. The resistive load is denoted by R_2. The constant power load power is known as PCPL. The CPS output current is also known as i_{CPS}. Define μ_2 as the power electronic switch S_2's duty cycle control amount. Kirchhoff's circuit rule allows the mathematical representation of the BESS in Figure 3 to be written as [22].

$$\begin{cases} C_{dc}\frac{dv_{dc}}{dt} = \mu_2 i_{L2} - i_{o2} \\ i_{o2} = \frac{v_{dc}}{R_2} + \frac{P_{CPL}}{v_{dc}} - i_{CPS} \\ v_g i_{L2} = v_{dc} i_d \end{cases} \quad (4)$$

Since S_2 and S_3 function in complementary conduction mode, the dynamic equation for the inductor current can be written as

$$L_2\frac{di_{L2}}{dt} = v_g + \mu_2 v_{dc} + R_{L2}i_{L2} \quad (5)$$

The BESS is charging and the converter operates in buck mode when S_3 is conducting. The BESS discharges and the converter operates in boost mode when S_2 is conducting. To ensure the stability of the DC bus voltage, the power electronic switch's PWM duty cycle is adjusted to regulate the BESS charging or discharging.

III. OPTIMAL CONTROL METHOD DESIGN

Due to the complicated operating conditions and time-varying, non-linear individual distributed source parameters in DC microgrids, it is challenging to sustain a constant condition throughout time. Therefore, it's critical to have a DC microgrid with reliable and steady operating control. The controller design of traditional PID control, a well-liked linear control technique, is based on a model that uses roughly linearization treatment close to the system equilibrium point, and the real control effect is subpar.

This study employs ISOA-PID control for BESS to achieve a good voltage robust control effect and variable step perturbation and observation method MPPT control to increase the operating efficiency of PV systems in accordance with the idea of maximum renewable energy usage.

A.PV system design of the MPPT controller

The relationship between the output power and output voltage, depicted in Fig. 4, is referred to as the PV cells' output characteristics. The V-I characteristics of the PV cell are nonlinear. Throughout the majority of the operating voltage range, the output Similar to the short-circuit current, the current is continuous. However, the current rapidly decreases when the output voltage approaches the open circuit voltage, resulting in a single-peak function with a maximum power point (MPP) for the output power characteristics. To boost the PV system's efficiency, PV cells should operate as close to the MPP as feasible. In actuality, though, the temperature and amount of sunlight fluctuate frequently. The idea behind maximum power point tracking is to use specific control devices and techniques to modify the equivalent input impedance in order to maximize the output power that the PV cells can produce. It is actually an independent optimization procedure [23–24].

The MPPT perturbation and observation approach is straightforward and simple to use. Nevertheless, it is sufficiently affected by the perturbation step size that it is unable to adjust to the shifting surroundings. When the perturbation step size is too tiny, the tracking speed is slow, and when the perturbation step size is too big, the voltage tends to oscillate. When the step size is far from the MPP, the exponentially variable step approach makes it larger; when it is near the MPP, it makes it smaller. Excellent tracking speed and accuracy can be attained with MPPT by combining the perturbation and observation method with an exponentially variable step method. The power variation exponential variable step perturbation and observation approach, which is accomplished by varying the duty cycle μ_1, serves as the foundation for MPPT control in this work. In contrast to the conventional fixed step perturbation and observation method, the suggested exponential variable step perturbation and observation method adds a time-varying smoothing factor m for the voltage increment ΔU. The distance from the MPP is correlated with the value of m, which ranges from 0 to 1. m assumes a significant value when the distance to the MMP is great. On the other hand, m assumes a tiny value. As a result, the step size ΔU is now a function of the time-varying coefficient m rather than a constant value [25]. As the operating point moves away from the MPP, the ΔP increment and the slope of the P-U characteristic curve both increase, as seen in Fig. 4. The incline While the operating point gets closer to the MPP, it gets smaller and the ΔP increment gets less. Depending on how ΔP varies the magnitude of the value of m changes. When ΔP is high, the m assumes a huge value that is very close to 1. m assumes a modest value when ΔP is small. This exponential function maps ΔP directly to the value of m. As ΔP varies, the value of m changes in real time and the expression is

$$m = 1 - \exp\left(-\|\Delta P\|^2\right) \tag{6}$$

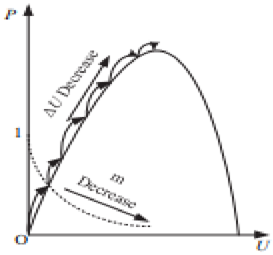

Figure 4: MPPT step change schematic diagram

Figure 5 illustrates the precise flow of the suggested exponential variable step perturbation and observation technique control. First, the technique calculates the U and I determines the value of ΔP and ΔU from the previous operating point at the current operating point. The step size at the subsequent operating point is then determined by taking the value of the time-varying factor m from the exponential function operation. By contrasting the voltage reference value U_{ref}*, the direction of disturbance of the specified voltage reference at the subsequent operating point, and the positive and negative values of ΔPΔU finally, at the next operating point, $=U_{ref} \pm m\Delta U$ are found.

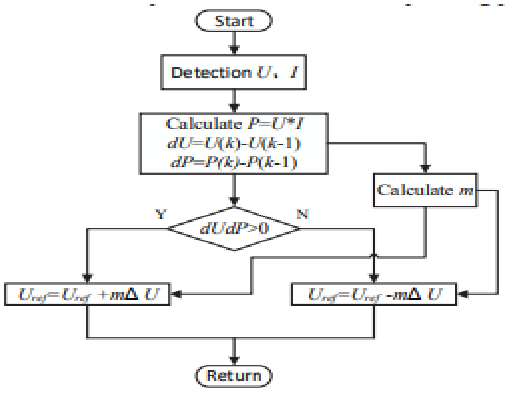

Figure 5 shows the flow of the suggested observation technique control and exponential variable step perturbation.

B.ISOA-PID voltage controller design for the BESS

PID controllers are frequently employed in DC microgrid control, and PID parameter optimization is a popular area of study to improve control effects. It's of excellent relevance for the BESS control system's fast responsiveness, stability, and dependability. The seeker optimization technique (SOA) is suggested in this research as a way to enhance and maximize PID controller performance. The absolute value of the error and the time integral of the squared control input term are set as the optimization target, while the PID parameters are specified as the search target.

Following recurrent search and computation, the system's ideal control quantity is then determined.

1).The analysis of the SOA principles

A novel kind of intelligent algorithm for human population behavior is called SOA. It considers the starting population to be the set total of search behaviors, and the behavior individuals as personal remedies. By mimicking human search patterns, the algorithm's inference judgment of position and direction is accomplished, and eventually the best solution to the issue can be found [26].

a) Fitness function selection: This study constructs the least objective function using the error absolute integral value in order to anticipate a suitable dynamic iterative property that will steer the algorithm to optimize toward the control objective. The definition of the created minimal objective function f is;

$$f=\begin{cases}\int_0^\infty \left[\eta_1\left|e(k)\right|+\eta_2 u^2(k)\right]dk, & e(k)\geq 0\\ \int_0^\infty \left[\eta_1\left|e(k)\right|+\eta_2 u^2(k)+\eta_3\left|e(k)\right|\right]dk, & e(k)<0\end{cases} \quad (7)$$

Where e(k) is the system error, u(k) is the control input, and η1, η2, and η3 are weights. Making $\eta_1>\eta_2$ and $\eta_1+\eta_2=1$ will satisfy the optimization requirements and lower the system error. Typically, To prevent overshoot, the penalty mechanism is applied, where $\eta_1=0.999$, $\eta_2=0.001$, and $\eta_3=100$.

b) Determining the size of the exploration step: SOA represents the search step fuzzy variables using the approximation function of the fuzzy system with a Gaussian subordination function, adhering to the seeker criteria.

$$u_A(x)=e^{-(x-u)^2/2\delta^2} \quad (8)$$

Where x is the input variable, u_A is the Gaussian affiliation, and u and δ are the affiliation function's parameters. The optimal position according to the linear affiliation function is to $u_{max}=1.0$, the maximum affiliation value. When the input exceeds [u-3δ, u+3δ], the affiliation is less than 0.0111, therefore it can be disregarded; that is, the worst position corresponds to the smallest affiliation, $u_{min}=0.0111$, and the other locations correspond to $0.0111<u<1$.

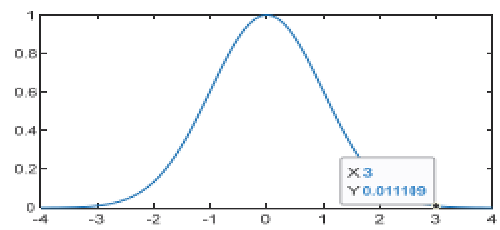

Figure 6: Distribution of Gaussian

$$u_{i,j}=rand\left(u_i,1\right)\left(j=1,2,\cdots,D\right) \quad (9)$$

Where D is the search space's dimension, $u_i$is the affiliation of the objective function value I, and $u_{i,j}$is the affiliation of the objective function value I in the j dimensional search space. Since the three are the optimization goal, PID settings, with D = 3.Step $a_{i,j}$ of the search is provided by;

$$\alpha_{i,j}=\delta_{i,j}\sqrt{-\ln\left(u_{i,j}\right)} \quad (10)$$

Where ui,j are the affiliation degrees of the search space objective function and $\delta_{i,j}$ are the parameters of the Gaussian affiliation function. The following determines its value: Formulas

$$\delta_{i,j}=\eta_0\times\left|x_{max}-x_{min}\right| \quad (11)$$

$$\eta_0=(T-t)/T \quad (12)$$

Where x_{max} and x_{min} are the locations of the population's maximum and minimum function values, and η0 is the inertia weight; T and t represent the highest quantity of iterations and the number of iterations that are currently in use, respectively.

c) Choosing the direction of the search: The egoist direction is d_e, the altruistic direction is d_a and the proactive direction is d_p, according to analytical modeling. They can be articulated as,

$$\begin{cases}\vec{d}_e(t)=\vec{p}_{best}-\vec{x}(t)\\ \vec{d}_a(t)=\vec{g}_{best}-\vec{x}(t)\\ \vec{d}_p(t)=\vec{x}(t_1)-\vec{x}(t_2)\end{cases} \quad (13)$$

Where x(t1) and x(t2) are the ideal positions in {x(t-2), x(t-1), x(t)}, respectively; p_{best} is the optimal position in individual history; and g_{best} is the global historical optimal location. A random weighted geometric average of the three directions is used to define the search direction d_f, and this can be written as,

$$d_f(t)=sign(\eta_0 d_p+m_1 d_e+m_2 d_a) \quad (14)$$

where m1 and m2 are real integers in the interval [0-1], and sign() is the sign function.

d) Individual location updates. The individual position update is performed following the acquisition of the search step $\alpha_{i,j}$and the search direction d_f. One way to express the revised position $x_{i,j}(t+1)$ is as

$$x_{ij}(t+1) = x_{ij}(t) + \alpha_{ij}(t) d_f(t) \quad (15)$$

2) The ISOA Algorithm

To address the issues of poor search efficiency in the early stages and the incapacity to locate the global optimal solution in the later stages of the SOA because of local extremum. Method [27], ISOA is suggested using the Cauchy variational operator and the chaotic initialization optimization technique The best performance is achieved by logistic chaos mapping, which can produce more symmetric and consistent random number distributions than square, sine, and other mappings. Thus, iteration is done iteratively using the logistic chaos mapping function [28–29].

$$x(\Phi+1) = \mu x(\Phi)[1 - x(\Phi)] \quad (16)$$

Where, is the number of iterations and μ is the parameter for regulation (0<1). The D-dimensional benchmark is generated at random. In the interval (0,1), particle y0, y0=(y01,y02,y03,…,y0H), the set of chaotic populations $y_{n+1,\,j}$ can be written as,

$$y_{n+1,j} = \mu y_{n,j}(1 - y_{n,j}) \quad (17)$$

The D-dimensional particle population x_{n+1}, j can then be obtained by mapping (0,1) onto the search space [-Γ, Γ], which can be written as

$$x_{n+1,j} = \Gamma \times (2 \times y_{n+1,j} - 1) \quad (18)$$

where N is the size of the population and D is the dimension of the search space; in this case, N=20 and D=3, and n = 0,1,2,…,N, j=1,2,…,D. The starting locations of the particle swarm that were acquired via the

The pre-search efficiency can be significantly increased by using the logistic chaotic mapping function in contrast to the initial positions determined by pseudo-random integers. Falling into local extreme in the latter stages of the search is addressed by the introduction of the Cauchy variational operator. The Gaussian distribution and the Cauchy distribution perform similarly, as Fig. 7 illustrates. The primary distinction is that the Cauchy distribution function's generated random numbers have a wider range of variances and longer wings. Therefore, the capacity to leap out of the As the algorithm position is updated, the local optimal solution gets stronger. [30–31] is the formula for the Cauchy variation.

$$A(t) = \begin{cases} x_{i,j}^t \times cauchy(0,1), rand(0,1) \le p \\ x_{i,j}^t, rand(0,1) > p \end{cases} \quad (19)$$

Where the usual Cauchy distribution function is Cauchy (0,1) and p is the random rate of variation.

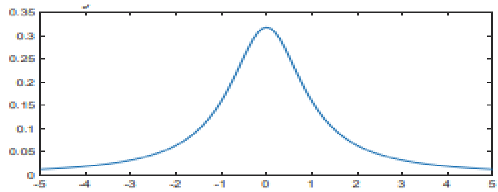

Figure 7. Cauchy distribution

Next, g_{best} is subjected to a mutation operation using the Cauchy distribution as

$$\begin{cases} g_{best,j}^{t+1} = g_{best,j}^t + \gamma \times A(t) \\ \gamma = e^{-\frac{\lambda t}{T}} \end{cases} \quad (20)$$

Where γ is the mutation weight; g_{best} ,j is the global optimal j dimensional component; λ is chosen as a constant, λ=10; T is the maximum number of iterations and t is the current number of iterations.

3) FEED-FORWARD CONTROLLER DESIGN BASED ON ISOA

Given that classical PID control's feed-back control method has a delay issue that might result in control failure or delay, a feed-forward compensating PID A control approach is suggested. The goal is to use feed-forward compensation to compensate PID in order to lower the system tracking error. Additionally, it may guarantee the system's quick reaction time and enhance the controller's tracking and control precision. Fig. 8 displays the principal block diagram.

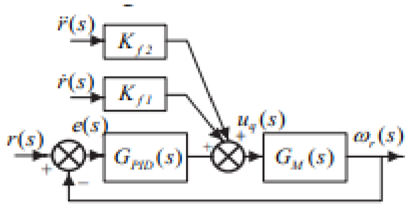

Figure 8: Feed-forward PID Controller Block Diagram

It is possible to express the system transfer function ωr(s)/r(s) and the system error transfer function e(s)/r(s) as;

$$\begin{cases} \dfrac{\omega_r(s)}{r(s)} = \dfrac{\left[G_{PID}(s) + K_{f1}\dot{r}(s) + K_{f2}\ddot{r}(s)\right]G_M(s)}{1 + G_{PID}(s)G_M(s)} \\ \dfrac{e(s)}{r(s)} = 1 - \dfrac{\left[G_{PID}(s) + K_{f1}\dot{r}(s) + K_{f2}\ddot{r}(s)\right]G_M(s)}{1 + G_{PID}(s)G_M(s)} \\ \quad = \dfrac{1 - \left[K_{f1}\dot{r}(s) + K_{f2}\ddot{r}(s)\right]G_M(s)}{1 + G_{PID}(s)G_M(s)} \end{cases} \quad (21)$$

Where GPID(s) is the PID transfer function under the Rasch transform, uq(s) is the voltage input under the Rasch transform, and r(s) is the initial input signal;

the speed tracking is e(s). Error under the Rasch transform the feed forward gain coefficients are K_{f1} and K_{f2}.

When K_{f1} r(s)+ K_{f2} r(s)=1/ G_m (s),Theoretically, the system error can be fixed. In actuality, the system error cannot be completely removed, but it can be decreased to a manageable level The photovoltaic-battery DC microgrid's robust control stability is significantly increased while minimizing any impact on system stability. PID discretization processing can be used to instantly transform a continuous system into a discrete system in situations when the PID sampling period TC is brief. Consequently, the discrete control law of feed forward compensated PID can be written as;

$$u_q(k) = K_p e(k) + K_i \sum_{l=0}^{k} e(l) + K_d\left(e(k) - e(k-1)\right) + K_{f1}\dot{r}(k) + K_{f2}\ddot{r}(k) \qquad (22)$$

Adjusting the parameters of a PID controller with a straightforward form and simple implementation is challenging for a photovoltaic-battery DC microgrid system with nonlinearity and hysteresis. Thus, self-tuning PID parameters based on ISOA is employed to accomplish system optimal control on a worldwide scale.

4) The Principle of ISOA-PID Control

The output speed tracking value and its ISOA-based feed-forward compensation PID control technique incorrect values are processed independently and optimized. Additionally, the controller's three parameters—K_p, K_i, and K_d—are changed to increase speed tracking precision and get rid of faults. Fig. 9 illustrates the control system principle.

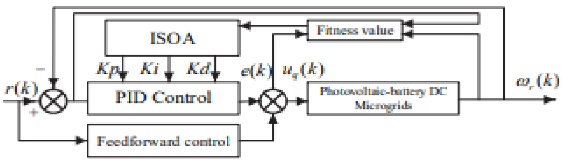

Figure 9: Control system principal diagram

The ISOA-PID control method works like this: Set the population and parameters to chaos. Adjust each particle's position and velocity. Assess each particle's fitness value and update the ideal position both locally and globally. Execute the global optimal Cauchy variation operation. Update and replace the population history ideal position after comparing it with the current individual optimal position. position if each person's present ideal job is superior. Output the ideal value and solution if the termination condition is met; if not, go back to step □. Fig. 10 displays the ISOA-PID flow chart.

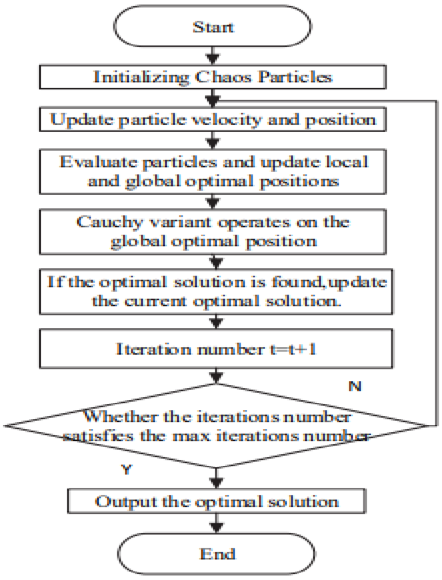

Figure 10. Flow chart for ISOA-PID

IV. ANALYSIS AND VERIFICATION OF SIMULATIONS

Simulation research using MATLAB/Simulink is utilized to confirm the efficacy and accuracy of the suggested control mechanism for photovoltaic-battery DC microgrid. The Table I displays the system parameters.

TABLE I

Circuit parameters of photovoltaic-battery DC microgrid

PV system parameters	Numerical values	*BESS* module parameters	Numerical values
Maximum power	10kW	Battery capacity	100Ah
Open-circuit voltage	37.2V	Open circuit voltage	300V
Short-circuit current	8.62A	C_g for standard values	1μF
Max. power voltage	30.2V	R_{L2} for standard values	100Ω
Maximum power current	8.1A	Standard values for L_2	0.01H

A. The PV system's control validation using the observation technique and exponential variable step perturbation

The PV system described in this study is made up of 50 PV cells, each of which can provide up to 200W of power at 1600 m2/W of sunshine. For MPPT simulation, pick one PV cell from the PV system. Set the temperature to 25°C and the initial solar intensity to 1400m2/W. The theoretical MPP under these circumstances is 177.77W. Decide on 0.1V as the step size for the typical disturbance observation. Figure 11 displays the simulation waveform diagram for both the conventional disturbance observation approach of the PV MPPT control and the exponential variable step perturbation and observation method. The exponential variable step disturbance observation method stabilizes in 10 ms, as illustrated in Fig. 11(a).

The conventional approach to disturbance monitoring stabilizes in 70 milliseconds. With amplitude changes of about 0.013W, the output power of the exponential variable step disturbance observation method stays constant between 177.757W and 177.77W, as illustrated in Fig. 11(b). Its ripple, when compared to the theoretical value, is 0.07. The conventional disturbance observation method has an amplitude fluctuation of 0.5W. Its ripple, in relation to the theoretical value, is 2.81 ‰. The PV system's energy loss is minimal with the suggested strategy, and its steady-state stability is high. For the PV system's MPPT control, it offers superior stability and speed.

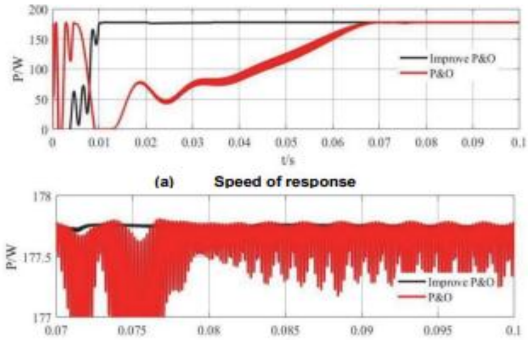

Figure 11. Comparison diagram for simulation

TABLE – ll

Comparison of MPPT control result with different methods

Method	Speed of response	Ripple value $((W_{max} - W_{min})/W_{theoretical})$
exponential variable step perturbation and observation	10ms	0.07‰
traditional disturbance and observation method	70ms	2.81‰

Assume that the outside temperature, T=25°C, stays the same. There are 1000W/m2 and 900W/m2 of sunlight. 800W/m2, with each phase being sustained for 0.2 seconds before being brought back to 1000W/m2. Figure 12 displays the PV system's MPPT simulation waveform with exponential variable step perturbation and observation technique.

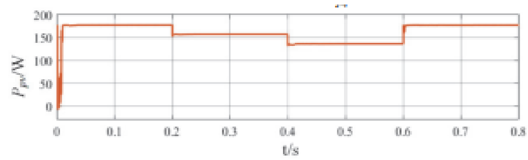

Figure 12: MPPT simulation with varying sunshine intensity and constant temperature

The suggested MPPT control approach exhibits outstanding response speed, steady-state stability, and dynamic transition process when the ambient temperature stays constant at T=25°C and the sunlight intensity varies at 0.2s, 0.4s, and 0.6s, respectively, as illustrated in Fig. 12.

B.ISOA-PID control for BESS is confirmed

The ISOA-PID controller's recommended parameters are Φ = 100, η1 = 0.999, η2 = 0.001, η3 = 100, m1 = 0.7, and m2 = 0.45. The conventional PID controller's ideal parameters are Kp = 0.03; Ki = 0.001; and Kd = 0.0002 [32].

1). STABILITY OF SUNLIGHT INTENSITY AND DEMAND FOR LOAD

First, suppose that the PV system is operating in a typical atmosphere with 1000 W/m2 of sunlight at first.a 25°C temperature, and a rated bus with V_{dc} = 600 V. In this scenario, the PV system's output power is less than the load, and it is assumed that the load demand and sunshine intensity remain constant. In order to meet the load demand, the PV system's DC-DC converter and the BESS's bi-directional DC-DC converter must work together to output power .According to Ohm's law, the load consumption at the start of the simulation is constant at PCPL = 3kW and iCPL = 5A. Figure 14(a)–(e) displays the load power consumption, DC bus voltage, and PV output power. Waveforms for the load current and BESS power input, respectively.

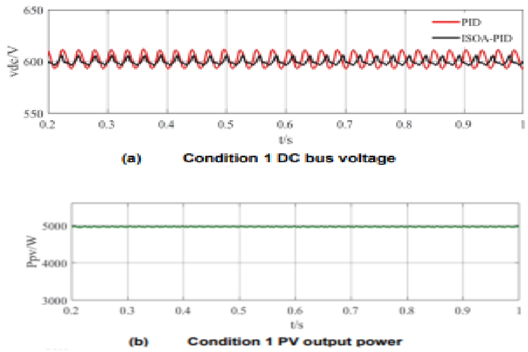

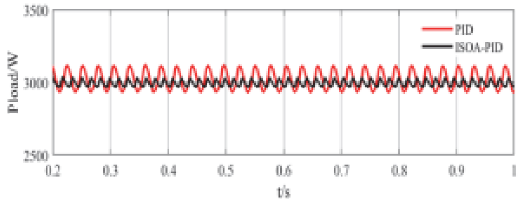

(c) Condition 1 load power consumption

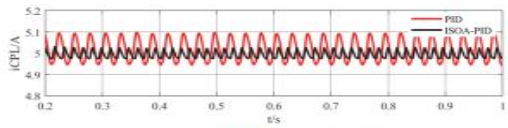

(e) Condition 1 load current

Figure 13. Microgrid output characteristics under condition 1

The DC micro grid's bus voltage is steady, as seen in Fig. 13(a). The PID-controlled bus voltage fluctuates, peaking at 611 V and falling to 592 V at its lowest. V. The ISOA-PID-controlled bus voltage oscillates between 606 V at its maximum and 597 V at its lowest. This demonstrates that compared to the PID, the ISOA-PID is more stable and oscillates less. The PV system reaches a steady state within 0.2 seconds, as seen in Fig. 13(b). According to the MPPT control algorithm, the maximum output power is kept at about 5kW, or P_{pv} = 5kW. The DC microgrid has no effect on the PV system's output power; only the temperature and amount of sunlight have an impact. The DC microgrid system's load power is demonstrated in Fig. 13(c), where the load power consumption reaches a steady state at 0.2s with a constant PCPL = 3kW. Achieves equilibrium with a load of 3kW. The ISOA-PID regulated the BESS's power waveform, as seen in Fig. 13(d). The BESS absorbs excess power from the PV system and serves as a power source to maintain the bus voltage. At 0.2 seconds, the BESS reaches a steady state. P_{bess} = -2kW and the BESS input power is kept at about 2kW. The PV power consumption and the power absorbed by the BESS add up to the load power consumption. Equation (1) states that the bus voltage is steady and produces the intended outcome when the net grid power P_{net}=0W. As illustrated in Fig. 13(e), the PID control's largest fluctuation value, iCPL = 5.1A, and lowest fluctuation value, iCPL = 4.95A, occur when the load current enters the steady state at 0.2s. ISOA-PID control has the lowest fluctuation value (iCPL = 4.97A), which is stable at roughly 5A, and the maximum fluctuation value (iCPL = 5.03A). The theoretical operation results from the simulation findings are in agreement with it. Table III displays the data from the simulation results mentioned previously. Under constant conditions, the suggested ISOA-PID control method outperforms the conventional PID control method in terms of suppressing load current fluctuations and stabilizing bus voltage oscillations.

TABLE III

Stability performance of two control methods under condition 1

Control method	Bus voltage			Load current
	Highest oscillation value	Lowest oscillation value	ripple percentage ((Vmax−Vmin)/Vavg)	ripple percentage ((Imax−Imin)/Iavg)
PID	611V	592V	3.2%	3.0%
ISOA-PID	606V	597V	1.5%	1.2%

2) STABILITY OF SUNLIGHT INTENSITY WITH VARIABLE LOAD POWER IS CONDITION 2.

Assume that the PV system's output power is less than the load, that the load power varies, and that the sunshine intensity remains constant. In this scenario, the PV system's DC-DC converter and the To satisfy the load demand, the BESS's bi-directional DC-DC converter must jointly output power The load consumption is fixed at PCPL = 3kW at the start of the simulation. After 0.5 seconds, the load consumption remains constant at PCPL = 8kW. Ohm's law states that the load current iCPL is equal to 5A prior to 0.5s and 13.33A thereafter to 0.5s. The DC bus voltage, load power consumption, BESS power input, and load current simulation waveforms are displayed in Fig.14, accordingly.

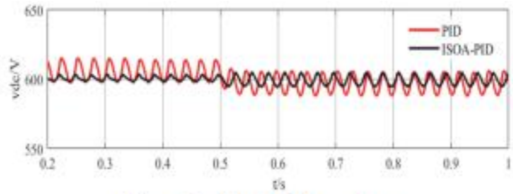

(a) Condition 2 DC bus voltage

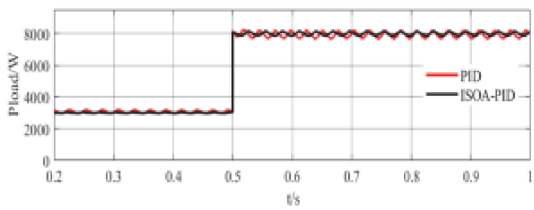

(b) Condition 2 load power consumption

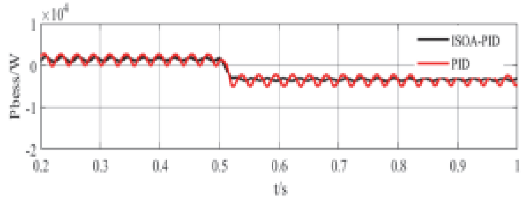

(c) Condition 2 BESS ISOA-PID control of input power

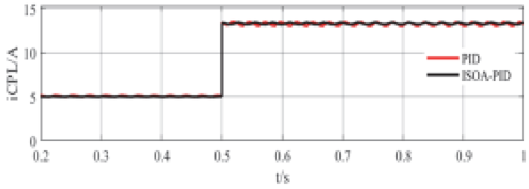

(d) Condition 2 load current waveform

Figure 14. Microgrid output characteristics in condition 2.

The PID DC microgrid's bus voltage is steady, as seen in Fig. 14(a). Prior to 0.5 seconds, 619V was the highest oscillation value and 599V was the lowest. After 0.5 seconds, 604V is the oscillation value at its highest, and 583V is at its lowest. Regarding the ISOA-PID, however, 602V is the maximum oscillation value prior to 0.5s. 599V is the lowest oscillation value. Following 0.5 seconds, 604V is the greatest oscillation value and 595V is the lowest. This suggests that ISOA-PID has a stronger control impact and is more stable than PID. With a constant load consumption of P_{CPL} = 3kW before 0.5s and a constant P_{CPL} = 8kW after 0.5s, P_{load} = 3kW, the power load reaches a steady state at 0.2s, as seen in Fig. 14(b). Before 0.5s and kept at P_{load} = 8kW after 0.5s, suggesting that the DC microgrid system's overall power is balanced.

The BESS power is utilized to absorb or make up for the PV system's excess or lack of power, as well as to keep the bus voltage steady, as seen in Fig. 14(c). The BESS reaches the steady state after 0.2 seconds, the output power is kept at about 3kW after 0.5 seconds, or P_{bess} = 3kW, and the input power is kept at around 2kW before 0.5 seconds, or P_{bess} = -2kW. The output power is rapidly switched, and the dynamic transition period is roughly 0.02 seconds. The total of the power supplied by the BESS and the PV output power is the load power consumption. Equation (1) states that the bus voltage is steady, the net grid power P_{net} = 0W, and the intended outcome is achieved. As illustrated in Fig. 14(d), the load current iCPL is 5A prior to 0.5s after the load current enters the steady state at 0.2s.

After 0.5 seconds, the load current iCPL is 13.3A. Control of ISOA-PID is less erratic in load current fluctuations and more stable than PID control. The PID-controlled load current iCPL reaches its maximum fluctuation value of 5.14A and its minimum fluctuation value of 4.97A, as illustrated in Fig. 14(e). In accordance with the theoretical simulate computation results, ISOA-PID-controlled load current iCPL obtains its peak fluctuation value of5.04A, lowest fluctuation value of 4.98A, and steady at roughly 5A. The PID-controlled load current iCPL reaches its maximum fluctuation value of 13.51A and its minimum fluctuation value of 13.10A, as illustrated in Fig. 14(f). ISOA-PID load control According to the findings of the theoretical simulation calculations, the current iCPL reaches its highest fluctuation value of 13.49A, its lowest fluctuation value of 13.20A, and its stable value of 13.33. Table IV displays the simulation results for working condition 2. According to the data analysis, the suggested ISOA-PID control approach outperforms the conventional PID control method in terms of controlling load current variation and bus voltage oscillation when sunlight intensity is constant and load demand varie

TABLE IV

Stability performance of two control methods under condition 2

Time	Control method	bus voltage			Load current
		Highest oscillation value	Lowest oscillation value	ripple percentage ((Vmax–Vmin)/Vavg)	ripple percentage ((Imax–Imin)/Iavg)
0.2s - 0.5s	PID	619V	599V	3.3%	3.4%
	ISOA-PID	602V	599V	0.5%	1.2%
>0.5s	PID	604V	583V	3.5%	3.1%
	ISOA-PID	604V	595V	1.5%	2.0%

3) CONDITION 3: THE INTENSITY OF THE SUNLIGHT AND THE POWER OF THE LOAD VARY 3) CONDITION 3: THE INTENSITY OF THE SUNLIGHT AND THE POWER OF THE LOAD VARY

Assume that the load demand and the amount of sunlight changes. In order to cooperatively modify the power to match the load demand, the PV system's DC-DC converter and the BESS's bidirectional DC-DC converter must charge and discharge. The load consumption is constant at PCPL = 3kW at the beginning of the simulation, and it remains constant at PCPL = 8kW after 0.5 seconds. Ohm's law states that the load current iCPL is equal to 5A prior to 0.5s and 13.33A thereafter to 0.5s. The solar intensity increases from 1000W/m2 to 1500W/m2 after 0.7s.The simulated waveforms for DC bus voltage, PV system output power, load power consumption, BESS input power, and load current are displayed in Fig. 15(a)–(c), accordingly.

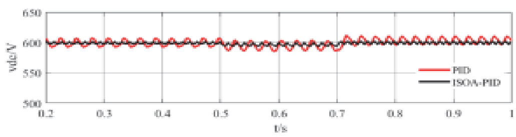

(a) Conditions 3 DC bus voltage

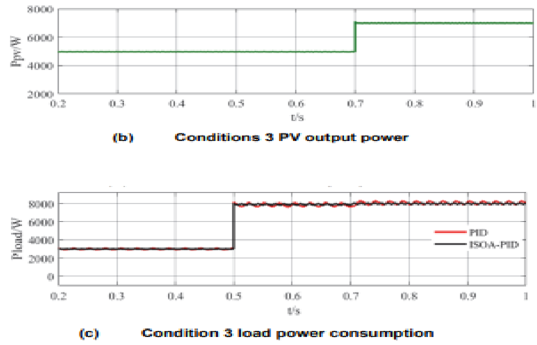

Figure 15. Microgrid output characteristics under condition 3.

The DC microgrid's bus voltage is steady, as seen in Fig. 15(a). There is significant fluctuation in the PID-controlled bus voltage oscillation; the maximum oscillation value is 605V, and the 595V was the lowest oscillation value between 0.2 and 0.5 seconds. Between 0.5s and 0.7s, the oscillation value ranges from 590V to 601V, which is the highest. After 0.7 seconds, the oscillation value ranges from 616V at its maximum to 598V at its lowest. In contrast, the ISOA-PID-controlled bus voltage fluctuates between 0.2 and 0.5 seconds at a minimum of 599V and a maximum of 601V. Between 0.5 and 0.7 seconds, the oscillation value ranges from 600V at its maximum to 596V at its lowest. After 0.7 seconds, the oscillation value reaches its maximum of 601V and its minimum of 598V.

The PV system enters the steady state at 0.2 seconds, as illustrated in Fig. 15(b), and maintains its maximum output power at about 5kW until 0.5 seconds, or P_{pv} = 5kW. After 0.7 seconds, it is kept at about 7kW, thus that P_{pv} = 7kW. The dynamic change happens quickly an smoothly. The DC microgrid has no influence on the total PV system's output power; only the temperature and intensity of the sun's rays do. The load power achieves the steady state at 0.2s, as illustrated in Fig. 15(c), with constant PCPL = 3kW prior to 0.5s and constant P_{CPL} = 8kW following 0.5s. For example, P_{load}= 3kW prior to 0.5s and keeps P_{load} = 8kW following 0.5s. The BESS is in a bi-directional flow state to maintain the bus voltage and compensate for or absorb the lack of load power from the PV system, as illustrated in Fig.15(d). The BESS reaches the steady state at 0.2s and is charging before 0.5s with power maintained at around 2kW, P_{bess} = -2kW. After 0.5s, it is discharging, where the output power is maintained from 0.5s to 0.7s at around P_{bess} = 3kW, and after 0.7s, the output power is maintained at around 1kW, P_{bess} = 1kW. According to equation (1), the net grid power P_{net} = 0W. The bus voltage is stable, and the anticipated outcomes are at the 0.5 and 0.7 second points, the shift is quick and seamless. According to Fig. 15(e), the load current iCPL is 5A before 0.5s and 13.3A after 0.5s once the load current achieves the steady state at 0.2s. Compared to the PID control, the ISOA-PID control is more stable and exhibits less fluctuation in the load current.The PID-controlled load current iCPL has the highest fluctuation value (i_{CPL} = 5.06A) and the lowest fluctuation value (i_{CPL} = 4.94A), as illustrated in Fig. 15(f). The ISOA-PID-controlled load current i_{CPL} stabilizes at about 5A, with the highest fluctuation value being 5.02A and the lowest fluctuation value being 4.98A.

PID-controlled load current i_{CPL} has a maximum fluctuation value of i_{CPL} = 13.41A and a minimum fluctuation value of i_{CPL} = 13.12A, as illustrated in Fig.15(g). There is a maximum fluctuation value for the ISOA-PID controlled load current i_{CPL}. Of i_{CPL} = 13.31A, with i_{CPL} fluctuating at a minimum of 13.20A before stabilizing at 13.33A. The PID-controlled load current i_{CPL} has the largest fluctuation value (i_{CPL} = 13.59A) and the lowest fluctuation value (i_{CPL} = 13.21A), as illustrated in Fig. 15(h). With a fluctuation value of 13.35A at its greatest and 13.26A at its lowest, the ISOA-PID-controlled load current i_{CPL} is stable at 13.33A. The theoretical calculation findings are followed by the simulation results above. Table V displays the results of these simulations. The data analysis demonstrates that the suggested ISOA-PID control method outperforms the traditional PID control method. in regulating load current fluctuations and bus voltage oscillations when load power and sunlight intensity fluctuate simultaneously

V. CONCLUSION

The key to guaranteeing the dependability of the power supply in a DC microgrid is robust and stable bus voltage regulation. The construction concept and bus voltage are examined in this work. The photovoltaic-battery DC microgrid is regulated. An ISOA-PID control approach is suggested for the bus voltage regulation and control requirement of BESS, while an enhanced exponential variable step perturbation and observation method is suggested for controlling its maximum power output. Simulation experiments show that, in comparison to the conventional perturbation and observation approach, the exponential variable step perturbation and observation method increased the reaction speed from 70 ms to 10ms. The amplitude of the output power fluctuation is reduced from 0.5W to 0.013W, thus it can be concluded that the proposed exponential variable step perturbation and observation method has the advantages of smaller energy loss, higher stability, and faster response. The stability performance of the voltage and current under conventional PID control and ISOA-PID control are also compared through simulation experiments with three different operating conditions. The average ripple percentage of its voltage and current decreases from 3% to 1%.

It concludes that ISOA-PID control can stabilize bus voltage oscillations and suppress load current fluctuations more effectively. Future research will examine a more sophisticated MPPT algorithm in partially shaded conditions to increase PV power generation efficiency. Additionally, the experimental hardware. A platform for more in-depth experimental study will be constructed.

REFERENCES

[1] Q. Xu, N. Vafamand, L. Chen, T. Dragičević, L. Xie and F. Blaabjerg, "Review on Advanced Control Technologies for Bidirectional DC/DC Converters in DC Microgrids," IEEE Journal of Emerging and Selected Topics in Power Electronics, vol. 9, no. 2, pp. 1205-1221, April 2021. DOI: 10.1109/JESTPE.2020.2978064.

[2] B. Aluisio, M. Dicorato, I. Ferrini, G. Forte, R. Sbrizzai, M. Trovato, "Planning and reliability of DC microgrid configurations for Electric Vehicle Supply Infrastructure," International Journal of Electrical Power & Energy Systems, vol. 131, 2021. DOI: 10.1016/j.ijepes.2021.107104.

[3] Ankan Chandra, G K Singh, Vinay Pant, "Protection techniques for DC microgrid- A review," Electric Power Systems Research, vol. 187, 2020. DOI: 10.1016/j.epsr.2020.106439.

[4] F. S. Al-Ismail, "DC Microgrid Planning, Operation, and Control: A Comprehensive Review," in IEEE Access, vol. 9, pp. 36154-36172, 2021. DOI: 10.1109/ACCESS.2021.3062840.

[5] Yang Mi, Jiahang Guo, Si Yu, Pengcheng Cai, Liang Ji, Yufei Wang, Dong Yue, Yang Fu, Chi Jin, "A Power Sharing Strategy for Islanded DC Microgrid with Unmatched Line Impedance and Local Load, " Electric Power Systems Research, vol. 192, 2021. DOI: 10.1016/j.epsr.2020.106983.

[6] Muhammad Mehdi, Saeed Zaman Jamali, Muhammad Omer Khan, Shazia Baloch, Chul-Hwan Kim, Robust control of a DC microgrid under parametric uncertainty and disturbances, Electric Power Systems Research, vol. 179, 2020. DOI: 10.1016/j.epsr.2019.106074.

[7] Manuela Sechilariu, Bao Chao Wang, Fabrice Locment, Antoine Jouglet, DC microgrid power flow optimization by multi-layer supervision control. Design and experimental validation, Energy Conversion and Management, vol. 82, pp. 1-10, 2014. DOI: 10.1016/j.enconman.2014.03.010.

[8] Y. Zheng, Y. Song, A. Huang, and D. J. Hill, "Hierarchical Optimal Allocation of Battery Energy Storage Systems for Multiple Services in Distribution Systems," in IEEE Transactions on Sustainable Energy, vol. 11, no. 3, pp. 1911-1921, July 2020. DOI: 10.1109/TSTE.2019.2946371.

[9] H. Kakigano, Y. Miura and T. Ise, "Distribution Voltage Control for DC Microgrids Using Fuzzy Control and GainScheduling Technique," in IEEE Transactions on Power Electronics, vol. 28, no. 5, pp. 2246-2258, May 2013. DOI: 10.1109/TPEL.2012.2217353.

[10] G. Bruni, S. Cordiner, V. Mulone, V. Rocco, F. Spagnolo, "A study on the energy management in domestic micro-grids based on Model Predictive Control strategies, " Energy Conversion and Management, vol. 102, pp. 50-58, 2015. DOI: 10.1016/j.enconman.2015.01.067.

[11] Dai Tengfei, Mao Jingfeng, Ding Yinjia, Yin Chunyun, Zhang Xiaotong, " Bus voltage stability control of the distributed photovoltaic and energy storage DC microgrid based on ADRC," in 2021 IEEE International Conference on Recent Advances in Systems Science and Engineering (RASSE), pp. 1-7, December 2021. DOI: 10.1109/RASSE53195.2021.9686941